THE JOURNAL OF PHYSICAL CHEMISTRY B

Article

pubs.acs.org/JPCB

Structural, Dynamical, and Electronic Properties of Liquid Water: A Hybrid Functional Study

Francesco Ambrosio,* Giacomo Miceli, and Alfredo Pasquarello

Chaire de Simulation à l'Echelle Atomique (CSEA), Ecole Polytechnique Fédérale de Lausanne (EPFL), CH-1015 Lausanne, Switzerland

ABSTRACT: We study structural, dynamical, and electronic properties of liquid water through *ab initio* molecular dynamics (MD) simulations based on a hybrid functional which includes nonlocal van der Waals (vdW) interactions. The water dimer, the water hexamer, and two phases of ice are studied as benchmark cases. The hydrogen-bond energy depends on the balance between Fock exchange and vdW interactions. Moreover, the energetic competition between extended and compact structural motifs is found to be well described by theory provided vdW interactions are accounted for. Applied to the hydrogen-bond network of liquid water, the dispersion interactions favor more compact structural motifs, bring the density closer to the experimental value, and improve the agreement with experimental observables such as radial distribution functions. The description of the self-diffusion coefficient is also found to improve upon the combined consideration of Fock exchange and vdW interactions. The band gap and the band edges are found to agree with experiment within 0.1 eV.

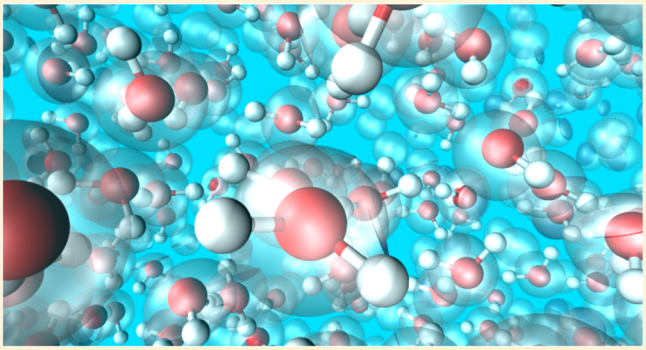

1. INTRODUCTION

Experimental and theoretical studies on liquid water represent a vast and fundamental research area, due to its central role in a plethora of biological and chemical processes.[1−3] From the perspective of computational physics, the study of structural, dynamical, and electronic properties of liquid water is also motivated by the challenges that the description of these physical observables pose to theory.[4]

Structural properties of liquid water have been investigated with both empirical force field[5,6] and *ab initio*[7−22] molecular dynamics (MD). The former method suffers from the dependence of the employed force fields on experimental data. The latter are mainly studies based on density functional theory (DFT) and strongly depend on the adopted exchange-correlation functional. Previous studies have shown that the generalized gradient approximation (GGA) yields radial distribution functions (RDFs) that are overstructured with respect to experiment.[7−15] This shortcoming of the GGA description of liquid water also affects the self-diffusion coefficient, which is largely underestimated.[16] Moreover, the equilibrium mass density, calculated from MD simulations in the isobaric isoenthalpic (NpH) ensemble[15] or by interpolating the pressures calculated from NVT simulations at different densities,[22] is found to be ∼15% lower than the experimental value.

The inclusion of Fock exchange through the use of a hybrid functional has been shown to produce contrasting results, depending on the adopted formulation.[16−22] Todorova et al. observed a slight improvement in the structural properties of liquid water, when using various hybrid functionals (PBE0,[23,24] B3LYP,[25] and X3LYP[26]), with small differences between them. At variance, the self-diffusion coefficient was found to be largely affected by the choice of hybrid functional, with the best estimates achieved with B3LYP and PBE0.[16] Guidon et al.[17] performed Born−Oppenheimer MD simulations of liquid water at the PBE,[27] HSE06,[28] and PBE0[23,24] levels of theory using the Gaussian plane-wave (GPW) method,[29] as implemented in the CP2K suite of codes.[30] They found little variation in the structural features when comparing these different functionals.[17] Moreover, a similar study found no evident correlation between the structural properties of liquid water and the fraction of Fock exchange introduced in the PBE0 functional.[18] In contrast, DiStasio et al. performed Car−Parrinello[31] MD simulations at the PBE0 level of theory, using a plane-wave basis set and a linear scaling algorithm.[32] They found a sensible improvement in the positions and heights of the peaks of the oxygen−oxygen RDF, when compared to the results obtained with PBE.[20] All these simulations were carried out in the NVT ensemble, thus providing no direct information on the equilibrium mass density of liquid water at the hybrid functional level of theory. Gaiduk, Gygi, and Galli calculated the equilibrium mass density of liquid water at the PBE0 level, and found it to be 0.71 g/cm^3, even lower than the PBE value. Moreover, the analysis of the RDFs revealed that the system was largely understructured.[22]

Received: April 16, 2016
Revised: July 12, 2016
Published: July 12, 2016

DOI: 10.1021/acs.jpcb.6b03876
J. Phys. Chem. B 2016, 120, 7456−7470

A fundamental improvement in the first-principles description of the structure of liquid water has been obtained with the inclusion of van der Waals (vdW) interactions in the exchange-correlation functionals. Different schemes have been proposed to account for these interactions.[33−41] Gaiduk, Gygi, and Galli used the Grimme dispersion corrections,[33] which enabled them to reproduce the experimental mass density, when used in conjunction with the PBE0 functional and temperature corrections.[22] Del Ben, Hutter, and VandeVondele employed the same scheme obtaining results very similar to those of highly accurate and computationally expensive methods, such as MP2[42,43] and the random phase approximation[44] (RPA).[19] The Tkatchenko−Scheffler scheme,[37] was employed by DiStasio et al., who recorded structural features in very good agreement with experiment.[20] Murdachaew, Mundy, and Schenter studied water clusters and liquid water using self-consistent polarization DFT, based on the BLYP functional.[41] They found an improved description of both cluster energetics and structural properties of liquid water, when compared to the parent BLYP functional.[41] Recently, Miceli, De Gironcoli, and Pasquarello showed that the nonlocal formulation of vdW interactions proposed by Vydrov and Van Voorhis,[40] in its revised form called rVV10,[45] grants a sensible improvement in the description of the structural and dynamical properties of liquid water when compared to results obtained with the PBE functional, without requiring any computational overhead.[15]

The electronic structure of liquid water has also been the subject of a large number of computational studies.[46−50] It is well-known that a poor description is achieved with GGA functionals, which generally tend to underestimate the electronic band gap of semiconductors and insulators.[51,52] For liquid water, the experimental band gap of 8.7 ± 0.6 eV[53] is underestimated by more than 4 eV at the PBE and BLYP[54,55] levels.[46,47,49] This poor result is mainly due to an incorrect description of the valence band edge, which is pushed toward higher energies by ∼3 eV, with respect to the experiment (at −9.3 eV with respect to the vacuum level).[48,56,57] At variance, the discrepancy of the conduction band edge with respect to experiment is found to be lower (0.5−0.6 eV), when compared with recent solvent polarization studies,[58] which situate this band edge at −0.5 eV with respect to the vacuum level. Standard hybrid functionals, such as HSE06 and PBE0, open the band gap (6.5 eV[46,47] and 7.2 eV,[49] respectively) but produce values which remain still quite far from experiment. Even the G_0W_0 description of the electronic structure of liquid water yields a band gap that is still ∼1 eV lower than experiment, due to an incorrect position of the VBM.[48] We have recently shown that the use of the PBE0 functional including 40% of Fock exchange on MD configurations achieved at the rVV10 level of theory leads to a band gap within 0.2 eV from experiment.[49] Moreover, the positions of the valence band maximum (VBM) and the conduction band minimum (CBM) when referred to the standard hydrogen electrode (SHE) were found to agree closely with recent experiments.[49] In the same work, we also showed that vdW interactions affect the band gap by only ∼0.1 eV.[49] Highly accurate results have been obtained using the self-consistent *GW* method with vertex corrections,[50,59] as accounted for by an approximated exchange-correlation kernel.[60] The calculations were performed using structural configurations obtained from MD simulations at the rVV10 level of theory. The quantum motion of the nuclei were taken into account through the path-integral MD formalism.[61] It was found that the inclusion of these effects causes a band gap renormalization of up to 0.6 eV due to hydrogen-bond fluctuations,[50] consistent with a previous study by Del Ben, Hutter, and VandeVondele.[19]

Achieving a correct description of the structural properties of liquid water does not grant that its electronic properties are well described at the same level of theory, as different physical effects influence the accuracy by which these properties are calculated. For this reason, electronic properties are often calculated using *GW* techniques or hybrid functionals on top of structural configurations achieved with MD simulations based on computationally less expensive methods.[48−50] Nevertheless, a simultaneous description of these physical observables would be desirable for the study of various chemical and physical phenomena in aqueous solution. For example, the studies of solvated species such as the radical water cation[62] and the solvated electron,[63] which show redox energy levels lying near the band edges,[62,64] require a proper description of the VBM and CBM of water in order to refer the calculated energy levels with respect to a physical reference, such as the SHE. Moreover, in order to achieve realistic MD trajectories for particular systems, it might be critical to overcome the limitations set by the self-interaction error implied in semilocal density functional descriptions.[65] Such improvements then need to be combined with the inclusion of vdW interactions, which are required to achieve a good description of the structure of liquid water.

In this work, we target a self-consistent description of the structural, dynamical, and electronic properties of liquid water at the hybrid functional level. We adopt a hybrid exchange-correlation functional including nonlocal vdW interactions. In particular, we use the PBE0 scheme with a fraction α of Fock exchange set to effectively reproduce the experimental band gap. Nonlocal vdW interactions are taken into account through the scheme proposed by Vydrov and Van Voorhis.[40,45] In this method, the analytic expression of the nonlocal electron correlation depends on an empirical parameter b, which governs the extent of the short-range interactions.[40,45] For the rVV10 functional, the optimal b parameter for liquid water has been inferred by varying b in MD simulations in the NpH ensemble. It has been found that the mass density and radial distribution functions are in closest agreement with experiment for b = 9.3.[15] In this work, we employ a similar procedure to optimize the b parameter for a hybrid functional, which results from the combination of the VV10 scheme with PBE0 (α = 0.40). We refer to this scheme as h-rVV10 and test its performance for the study of three benchmark cases: (i) the water dimer, (ii) the water hexamer, and (iii) the comparison between two phases of solid water: ice I_h and ice VIII. We find that the hydrogen-bond energy depends on the interplay between Fock exchange and the extent of the vdW interactions. The latter are shown to provide an increase in the hydrogen-bond energy, which compensates for the low value resulting from the use of a hybrid functional. Moreover, we observe that the inclusion of vdW interactions plays a fundamental role in balancing the competition between extended and compact structural motifs, the stability of the latter being strongly underestimated by standard semilocal and hybrid functionals.

Hence, we study the structural, dynamical, and electronic properties of liquid water. We observe that the low density induced by the use of Fock exchange in the hybrid functional is counteracted by vdW interactions favoring more compact configurations. We find optimal parameters for the hybrid functional leading to a mass density and structural features in

DOI: 10.1021/acs.jpcb.6b03876
J. Phys. Chem. B 2016, 120, 7456−7470

good agreement with experiments. We find that both Fock exchange and dispersion interactions contribute to enhancing the mobility of the water molecules, sensibly improving the self-diffusion coefficient. The band gap and the band edges agree within 0.1 eV with their experimental counterparts, when referred to the SHE level.

This paper is organized as follows. In section 2, we present the hybrid functional including nonlocal vdW interactions introduced in this work and analyze its performance for three test cases: (i) the water dimer, (ii) the water hexamer, and (iii) ice I_h and ice VIII. In section 3, we carry out DFT-MD simulations of liquid water based on the present hybrid functional and describe the resulting structural, dynamical, and electronic properties. The conclusions are drawn in section 4.

2. BENCHMARK OF HYBRID FUNCTIONALS

All the calculations performed in this work are carried out at the hybrid functional level of theory. In particular, we employ the PBE0 functional[23,24] and include nonlocal electron correlation via the scheme conceived by Vydrov and Van Voorhis, in the revised form proposed by Sabatini et al.[40,45] The employed functional is referred to as h-rVV10 and has the following form:

$$E_{xc}^{\text{h-rVV10}} = \alpha E_x^{F} + (1-\alpha)E_x^{PBE} + E_c^{PBE} + E_c^{nl} \quad (1)$$

where α is the fraction of Fock exchange E_x^F, E_x^{PBE} the PBE exchange, and E_c^{PBE} the PBE correlation, and E_c^{nl} accounts for the nonlocal vdW interactions within the Vydrov and Van Voorhis scheme.

Recent studies already focus on various schemes to account for vdW interactions providing similar results among them.[33−41] The choice of combining the rVV10 scheme with the PBE0 functional is here motivated by the consideration that this scheme can be easily optimized in conjunction with the hybrid functional. This can be achieved by tuning the b parameter which controls the extent of the short-range interactions in the analytical expression of E_c^{nl}.[40]

In this work, we set $\alpha = 0.40$, which has been found in ref 49 to give a good description of the electronic structure of liquid water, including its band gap, band edges, and redox levels, when employed on structural configurations resulting from MD simulations based on rVV10.[49] we remark that our choice of α aims at reproducing the experimental band gap in MD simulations in which the nuclear motions are treated classically. In case an explicit treatment of the quantum motion of the nuclei is envisaged, a higher value of α should be considered in order to account for the expected band gap renormalization.[19,50] We here refer to PBE0(0.40) and h-rVV10 as to functionals in which α is set to 0.40, unless specified differently. For the optimization of the b parameter in h-rVV10, we test in the following four different values: 9.3, 6.3, 5.8, 5.3.

Interestingly., a similar value of α, 0.38, was employed in the PBE38 functional and used in conjunction with Grimme dispersion corrections in the study of thermochemistry, kinetics, and noncovalent interactions for benchmark sets.[66,67] We underline that the energetics and electronic properties of condensed phase systems are mostly preserved when the fraction of Fock exchange is varied. This has been shown both for defects in crystalline materials[68,69] and for redox levels in aqueous solution.[49]

We use the freely available CP2K package, which takes advantage of an atomic-orbital basis set for the wave functions and of a plane-wave expansion for the electron density.[29,30] We use a triple-ζ polarized basis (TZV2P) set derived from the all-electron basis set presented in ref 70 and optimized to be used in conjunction with pseudopotentials. We employ a cutoff of 800 Ry for the plane-wave expansion. The performance of this basis set for simulations of liquid water has been found to be comparable with that of a DFT code based on plane waves basis sets,[15,71] such as QUANTUM ESPRESSO.[72] The analytical Goedecker−Teter−Hutter pseudopotentials are used to describe core−valence interactions.[73,74] Standard convergence criteria are used for the optimization of the wave functions: 10^{-7} au for the electronic gradient and 10^{-12} au for the energy difference between the final self-consistent field (SCF) cycles. Fock exchange is treated using the auxiliary density matrix method (ADMM),[17,75,76] which allows for a rapid evaluation of the exchange integrals through the use of a smaller auxiliary basis set. In this work, we employ the cFIT3 auxiliary basis set.[17,75,76] The use of an atomic basis set in the calculation of binding energies is affected by the basis set superposition error (BSSE).[77] This has been taken into account in this work via the counterpoise scheme developed by Boys and Bernardi.[78] The BSSE corrections applied to the dimer binding energies are smaller than 0.02 eV.

2.1. Water Dimer. The binding energy of the water dimer, $E_b[(H_2O)_2]$, is a convenient benchmark for testing theoretical schemes developed for studying liquid water.[79,80] In fact, this provides an estimate of the hydrogen-bond strength, which is a fundamental quantity in the description of water in condensed phases.[81] In Table 1, we report values for the dimer binding energy as obtained with the h-rVV10 functional with two different values of b: 9.3 and 5.3, along with the result calculated at the PBE0(0.40) level. We also report previous results obtained with PBE and rVV10.[15] In the calculations, we use the geometry of the water dimer as it has been optimized at the coupled cluster level of theory including single, double, and triple excitations [CCSD(T)] in the complete basis set limit.[82] The binding energy achieved at this level of theory is taken as reference value.[82]

Table 1. Binding Energy of the Water Dimer $E_b[(H_2O)_2]$ (eV) as Calculated at Various Levels of Theory, in Comparison with Previous Studies[15,82]

theory	$E_b[(H_2O)_2]$
reference: CCSD(T)[82]	0.22
PBE[15]	0.22
rVV10-b9.3[15]	0.23
rVV10-b6.3[15]	0.25
PBE0(0.40)	0.18
h-rVV10-b9.3	0.20
h-rVV10-b5.3	0.22

Among the studied approaches, PBE0(0.40) provides the lowest value of $E_b[(H_2O)_2]$, which explains the weaker hydrogen-bond network previously encountered in simulations of liquid water at this level of theory.[16,22] We notice that vdW interactions produce an increase of $E_b[(H_2O)_2]$ when they are added to the GGA or to the hybrid functional. The nice agreement between the PBE and CCSD(T) should not be considered satisfactory. In fact, it is known that $E_b[(H_2O)_2]$ is well reproduced by the PBE functional, due to the exchange-enhancement factor suppressing spurious exchange attraction.[4] However, the lack of vdW interactions leads to a complete failure of this functional, when considering larger clusters and

DOI: 10.1021/acs.jpcb.6b03876
J. Phys. Chem. B 2016, 120, 7456−7470

condensed phases, as shown in the next sections. Indeed, the agreement with the reference CCSD(T) value deteriorates when considering rVV10. At variance, the PBE0(0.40) value underestimates the hydrogen-bond strength and the inclusion of vdW interactions as achieved with h-rVV10-b5.3 brings the calculated binding energy in agreement with the CCSD(T) reference.

2.2. Water Hexamer. A second benchmark of the performance of exchange-correlation functionals in the description of liquid water is the study of the binding energy of the isomers of the water hexamer, $(H_2O)_6$. In particular, we focus on two different clusters, the ring-shaped and the prism-shaped ones. The ring-shaped hexamer (cf. Figure 1a)

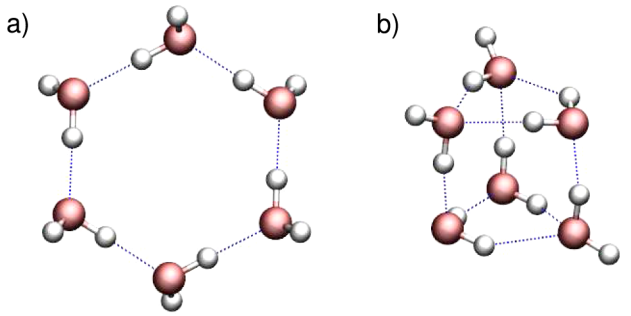

Figure 1. Ring-shaped (a) and prism-shaped (b) isomers of the $(H_2O)_6$ cluster. Oxygen atoms in red, hydrogen atoms in white.

possesses six hydrogen bonds, all of them being similar to the one encountered in the dimer. Oppositely, the geometry of the prism-shaped hexamer (cf. Figure 1b) allows the formation of nine distorted hydrogen bonds. The competition between a more extended structure with regular hydrogen bonds and a more packed configuration with weaker hydrogen bonds governs the difference between the binding energies of these two isomers. Therefore, it is evident that this test case provides a clear assessment of the relevance of dispersion interactions.

CCSD(T) calculations indicate that the prism-shaped isomer is more stable than the ring-shaped one, even if the difference is very small (~0.01 eV,[83] cf. Table 2). The same ordering has

Table 2. Calculated $E_b[(H_2O)_6]$ (eV) in this Work and in Previous Studies[83]

theory	ring	prism
reference: CCSD(T)[83]	0.32	0.34
PBE	0.37	0.36
rVV10-b9.3	0.37	0.38
PBE0	0.31	0.29
PBE0(0.40)	0.27	0.23
h-rVV10-b9.3	0.29	0.27
h-rVV10-b5.3	0.30	0.32

also been achieved with diffusion Monte Carlo and MP2 calculations.[84,85] In contrast, standard GGA and hybrid functionals were found to fail in reproducing the correct ordering between these isomers, mainly due to the lack of dispersion interactions.[86]

We calculate the binding energy per water molecule of ring-shaped and prism-shaped hexamer clusters ($E_b[(H_2O)_6]$), on structural configuration achieved at the CCSD(T) level of theory.[83] The results listed in Table 2 indicate that the PBE functional is unable to describe the correct ordering among the two isomers, in agreement with previous calculations.[86] The use of a hybrid functional affects the binding energies of both clusters, which are found to decrease as a function of the fraction of Fock exchange α introduced in the PBE0 functional. Moreover, the difference of the binding energies of the prism-shaped and ring-shaped clusters increases with α, with the ring-shaped isomer being 0.02 and 0.04 eV more stable than the prism structure when α is set to 0.25 and 0.40, respectively. The introduction of dispersion interactions enables us to recover the correct ordering between isomers, for both the rVV10-b9.3 and h-rVV10-b5.3.

2.3. I_h Phase of Ice and Ice VIII. A third benchmark case for the adopted hybrid functional is the study of ice. In particular, we investigate physical properties of (i) the I_h phase of ice and (ii) ice VIII. The former corresponds to the common ice phase at ambient conditions and is studied through the model proposed by Bernal and Fowler,[87] which has been extensively employed to test the accuracy of density functionals in the description of hydrogen-bond networks in ice.[15,88−90] The latter is a compressed proton-ordered tetragonal structure which forms at low temperatures and high pressure (>2 GPa).[91] Notwithstanding the huge compression, which results in an equilibrium volume being lower by ~37% than that of ice I_h, it is experimentally determined that the sublimation energy per molecule of ice VIII is lower than that of ice I_h by only ~0.03 eV.[92] Standard semilocal functionals and hybrid functionals completely fail in capturing this trend, as the sublimation energy of ice VIII is found to be lower than that of I_h ice by over 0.1 eV.[90] Therefore, a comparison between ice I_h and ice VIII allows us to analyze the effect of vdW interactions on extended and compact structural configurations in the condensed phase.

The calculations of the I_h phase of ice are performed through the use of an orthorhombic supercell of 96 water molecules, built from the hexagonal unit cell, as proposed in ref 93 (cf. Figure 2a). Ice VIII is modeled with an orthorhombic supercell

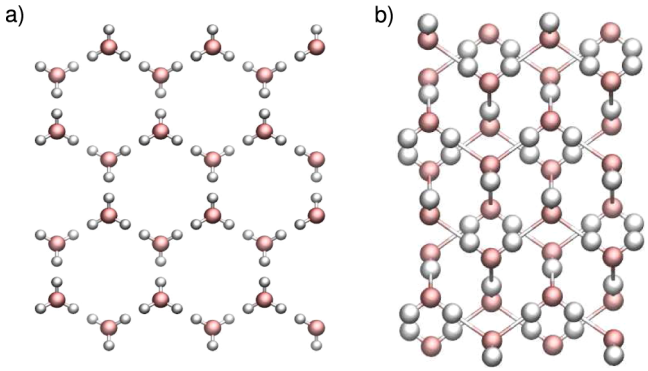

Figure 2. Representation of the orthorhombic supercell used to simulate (a) the I_h phase of ice and (b) ice VIII. H atoms in white, O atoms in red.

containing 64 water molecules (cf. Figure 2b). All the calculations are performed with a **k**-point sampling consisting of the sole Γ point. The basis set, the pseudopotentials, and the convergence criteria are the same as specified at the beginning of section 2.

In order to evaluate sublimation energies per molecule (E_{sub}), bulk moduli (B_0), and equilibrium volumes per molecule (V_0), we perform calculations at various fixed volumes. Moreover, in order to ensure that all the hydrogen bonds have the same

DOI: 10.1021/acs.jpcb.6b03876
J. Phys. Chem. B 2016, 120, 7456−7470

length and to avoid the formation of dipoles, we set the lattice constant ratio a/c to the ideal face-centered cubic value, as proposed in ref 88, for all employed supercells. The calculated energies are fitted by a Murnaghan equation of state (cf. Figure 3).[94] Derived values for E_{sub}, V_0, and B_0 are reported in Table 3.

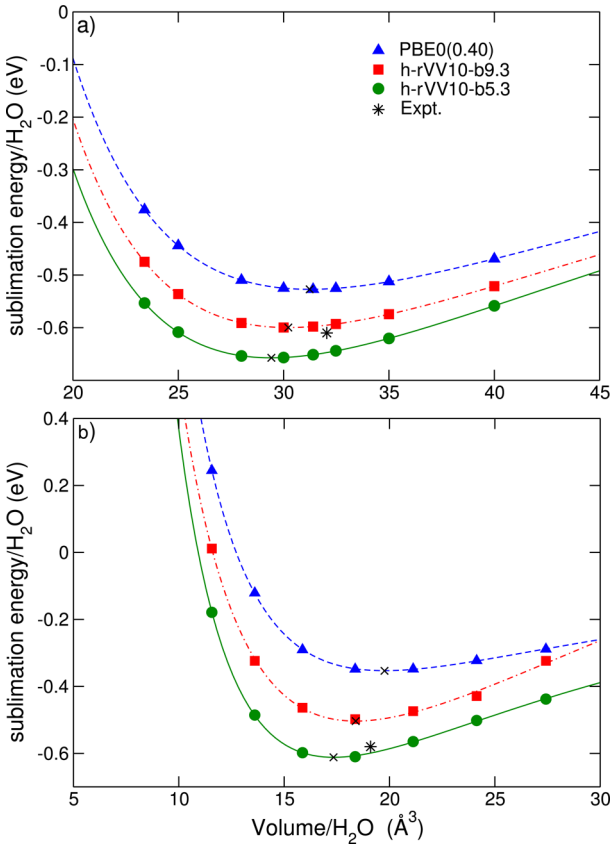

Figure 3. Sublimation energies per H_2O molecule vs volume per H_2O molecule for (a) ice I_h and (b) ice VIII, as obtained with PBE0(0.40), h-rVV10-b9.3, and h-rVV0b5.3. The minima of the fitted Murnaghan equation of state are indicated. The experimental values from ref 92 (asterisks) are reported for comparison.

Table 3. Calculated Values of E_{sub} (eV), B_0 (GPa), and V_0 (Å^3) for the I_h Phase of Ice and Ice VIII, Compared to Experiment[91,92,95,96]

	E_{sub}	V_0	B_0
	I_h Ice		
PBE0[22,90]	0.60	31.33	13.0
PBE0+vdW[90,a]	0.67	29.88	
PBE0(0.40)	0.53	31.23	13.2
h-rVV10-b9.3	0.60	30.22	14.2
h-rVV10-b5.3	0.65	29.41	16.0
expt[91,92,95]	0.61	32.05	10.9
	Ice VIII		
PBE0[90]	0.45	20.27	
PBE0+vdW[90,a]	0.60	19.7	
PBE0(0.40)	0.35	19.76	15.72
h-rVV10-b9.3	0.50	18.39	26.76
h-rVV10-b5.3	0.61	17.34	28.2
expt[92,96]	0.58	19.1	27.9

[a]vdW interactions are accounted for via the Tkatchenko−Scheffler scheme.[37]

PBE0(0.40) underestimates the sublimation energy of I_h ice by 0.08 eV (roughly by 0.04 eV per hydrogen bond, cf. Table 1), a consequence of the weak hydrogen-bond strength at this level of theory. However, the underestimation of the sublimation energy per molecule of ice VIII is even larger (0.23 eV), as a consequence of the treatment of a more compact structure and the absence of vdW interactions. Calculations including vdW interactions provide a better agreement with experiment. The values of V_0 and B_0 derived with PBE0(0.40) are closer to experiment than upon the consideration of vdW interactions for ice I_h. A similar deterioration of V_0 and B_0 has previously been encountered in ref 15 when going from PBE to rVV10. Similar results for ice I_h were also obtained in ref 90 when using PBE0 in conjunction with vdW interactions described through the Tkatchenko−Scheffler scheme.[37] Nevertheless, the bulk modulus of ice VIII reaches its experimental counterpart within only 0.3 GPa for h-rVV10-b5.3. However, equilibrium volumes are still underestimated when vdW interactions are accounted for. We observe that the difference between the sublimation energies of ice I_h and ice VIII as calculated with h-rVV10-b5.3 approaches the experimental estimate.

3. MOLECULAR DYNAMICS SIMULATIONS OF LIQUID WATER

3.1. Computational Details. In order to evaluate the equilibrium mass density of liquid water at different levels of theory, we perform *ab initio* Born−Oppenheimer MD simulations in the isobaric isothermal ensemble (NpT) on a periodic supercell of cubic shape containing 64 water molecules. The target temperature is set to 350 K and is controlled by a Nosé−Hoover thermostat.[97,98] In our NpT simulations, the cell dimension is allowed to fluctuate with the only constraint of retaining the initial cubic symmetry. The external pressure is controlled via the barostat developed by Martyna, Tobias, and Klein.[99] MD simulations are performed at the PBE0(0.40) and h-rVV10 levels of theory, with the latter being carried out at the following values of b: 9.3 (which was found to give the best description of the structural properties of liquid water at the semilocal level),[15] 6.3 (the original value),[40] 5.8, and 5.3. For each value of b, MD simulations are run for 25−35 ps, with a time step of 0.48 fs. Basis sets, pseudopotentials, and convergence criteria are the same as in section 2. Since `CP2K` features a plane-wave basis set to re-expand the electron density, a fluctuation of the volume produces a fluctuation of the number of grid points in the calculations. For this reason, we employ a supercell with a density of 1 g/cm^3 as starting geometry for h-rVV10 MD simulations. For PBE0(0.40) a starting geometry at a smaller value of density (0.86 g/cm^3) is employed. The plane-wave basis set is then defined through a reference cell with a larger side to ensure that the plane-wave expansion still gives a converged expansion upon the increase of volume during the simulation.

In order to calculate the self-diffusion coefficient of water, we perform MD simulations at the experimental density in the NVE ensemble for both PBE0(0.40) and h-rVV10-b5.3. We first carry out equilibration runs in the NVT ensemble for 30 ps. Hence, we turn off the thermostat and proceed with a 20 ps MD simulation in the NVE ensemble. No significant drift in the temperature is observed during these MD runs.

The absence of any significant computational overhead associated with the use of the rVV10 scheme has already been

DOI: 10.1021/acs.jpcb.6b03876
J. Phys. Chem. B 2016, 120, 7456−7470

verified for a plane wave based DFT code.[15,45] We find that this consideration also applies to CP2K, leading to an overhead of less than 2%.

In our simulations, we use a temperature of 350 K for two main reasons. First, with respect to 300 K, this temperature favors liquid-like behavior of liquid water simulations.[11,12] Previous simulations at the semilocal level have shown indications of glassy behavior.[11] Given the heavy computational cost of hybrid functional calculations, it is advised to avoid temperatures at which the simulated systems would fail in reproducing a frank diffusive motion. Moreover, choosing a temperature of 350 K allows us to directly compare our results with previous studies based on semilocal density functionals,[15,49] but otherwise following the same protocols as in the present work. This allows us to clearly isolate the effect of adopting a hybrid functional scheme. We remark that experimental radial distribution functions undergo only minor variations between 300 and 350 K.[100] The change is negligible for the first peak in the oxygen−oxygen radial distribution function. For the height of the second peak, the variation amounts to about 25% of the difference we observe between experiment and theory (*vide infra*). In the following, it is therefore justified to confront radial distribution functions obtained from simulations at 350 K with experimental data recorded at ambient temperature. It should be noticed that a thermal difference of 50 K corresponds to an energy difference of ∼4 meV, which is still very challenging in the theoretical description of water systems (cf. section 2).

In this work, we do not account for nuclear quantum effects (NQEs). While previous studies suggested that these effects could affect the structure in a similar way as a small temperature increase,[101] this view has recently been questioned and NQEs have remained a matter of debate.[102] For instance, it has become clear that NQEs depend on the structure achieved with the adopted electronic structure scheme.[102] Recent path-integral results for semilocal functionals including vdW interactions,[103,104] which could be considered to yield structural properties similar to those achieved in the present work with hybrid functionals, are barely affected by the explicit treatment of NQEs. In particular, the height of the first peak in the oxygen−oxygen radial distribution is slightly reduced, the second minimum is barely deepened, and the height of the second peak is lightly increased. Since all these changes are significantly smaller than the differences we observe between experiment and theory (cf. section 3.3), NQEs can be neglected for the purpose of the present work.

3.2. Equilibrium Mass Density. In contrast with simulations in the NVT ensemble that require a series of MD runs at different densities, a single NpT MD simulation allows one to directly evaluate the equilibrium mass density, obtained as an average over the MD run. The convergence of the mass density with respect to the simulation length is illustrated in Figure 4a. The statistical errors are determined taking into consideration the correlation time of density-density correlations (∼1.6 ps). At the PBE0(0.40) level, we find that the equilibrium mass density is largely underestimated (0.56 g/cm^3, cf. Figure 4b). PBE(0.40) underestimates the experimental value even more than PBE (0.87 g/cm^3, cf. ref 15). Moreover, the obtained density is lower by 0.15 g/cm^3 than the value found in ref 22 with PBE0. This result suggests that the larger the fraction of Fock exchange, the larger the decrease in the equilibrium mass density.

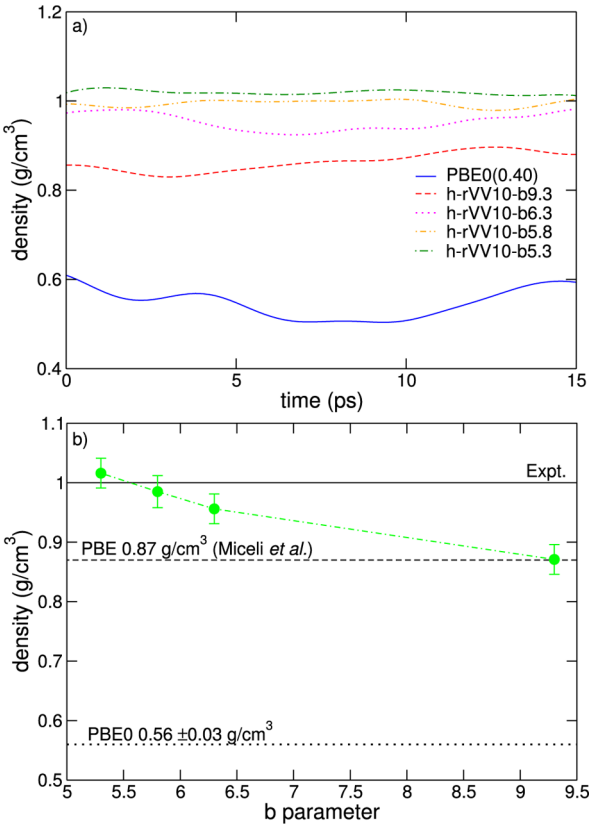

Figure 4. (a) Mass density as a function of simulation time for the last 15 ps of each MD run. A Gaussian broadening of 1 ps is employed. (b) Equilibrium mass density as a function of the parameter b defining the h-rVV10 functional. Black solid line for the experimental value, black dashed line for the PBE value of ref 15, and black dotted lined for the value calculated in this work with PBE0(0.40). The green line is drawn only to guide the eye.

h-rVV10 simulations including nonlocal vdW interactions produce higher densities. However, the b value of 9.3, which was found to be optimal for liquid water when the rVV10 scheme is combined with a semilocal functional,[15] only gives a density of 0.87 g/cm^3 when combined with the hybrid functional, resulting in a similar deviation from experiment as plain PBE.[15] For b = 5.8 and b = 5.3, we find equilibrium densities of 0.98 and 1.02 g/cm^3, respectively, both agreeing with experiment within 0.02 g/cm^3.

In the interpretation of structural variations upon the modification of the external thermodynamic conditions, an important role is commonly attributed to rearrangements in the hydrogen-bond network formed by the water molecules.[105,106] It is therefore of interest to understand how density variations relate to modifications of the hydrogen-bond network. Our study shows that higher densities cannot trivially be attributed to a disruption induced by a diminished hydrogen-bond strength. On the contrary, the consideration of nonlocal vdW interactions produces stronger hydrogen bonds (cf. Table 1), while the density nevertheless increases. This behavior can be rationalized by distinguishing between the directional and nondirectional bonding induced by the hydrogen bond and the vdW interactions, respectively. As the vdW interactions increase, the nondirectional bonding becomes favored, leading to the stabilization of more compact configurations, which would otherwise remain unfavorable.[15] The resulting rearrangements dominate the structural organization, and the slight

DOI: 10.1021/acs.jpcb.6b03876
J. Phys. Chem. B 2016, 120, 7456−7470

increase in the dangling bond energy of the dimer should only be considered as a minor side effect. This is also related to what has been observed in the comparison of the different hexamer clusters and ice phases. In the next two sections, we analyze the structural reorganization induced by the vdW interactions through the study of the radial distribution functions and of the hydrogen-bond network.

3.3. Radial Distribution Functions. The radial distribution functions represent a clear benchmark for examining the structure of liquid water in the simulations against recent X-ray diffraction and neutron scattering experiments performed at ambient temperature (295−300 K).[107−109] In Figure 5a, the oxygen−oxygen radial distribution functions obtained with various functionals are compared with the most recent experimental X-ray diffraction data of ref 107 recorded at 296−300 K. The results clearly indicate that liquid water achieved with PBE0(0.40) is very different from the experiment, consistent with the PBE0 results obtained in ref 22. In particular, the first minimum and the second peak of the RDF are noticeably shifted toward higher distances, a consequence of the low density achieved at this level of theory. The introduction of dispersion interactions through the rVV10 scheme increases the density of liquid water, and, consequently, the peaks and the minima of the RDF move closer to the experimental positions. However, for b = 9.3, we still find significant overstructuring, as can be inferred from the height of the RDF in correspondence of the first minimum and of the second peak. This indicates that directional bonding still dominates the network formation leading to a RDF which overall resembles the one obtained with plain PBE.[15] Upon further decrease of b to 5.3, we find a much better agreement with experiment, comparable to the one achieved with the rVV10-b9.3 functional.[15] In particular, the positions of the first and the second peak of the RDF agree with experiment within 0.05 and 0.2 Å, respectively. Only a slightly larger difference still persists for the position (3.3 Å vs 3.5 Å in the experiment) and height (0.61 vs 0.79 in the experiment) of the first minimum.

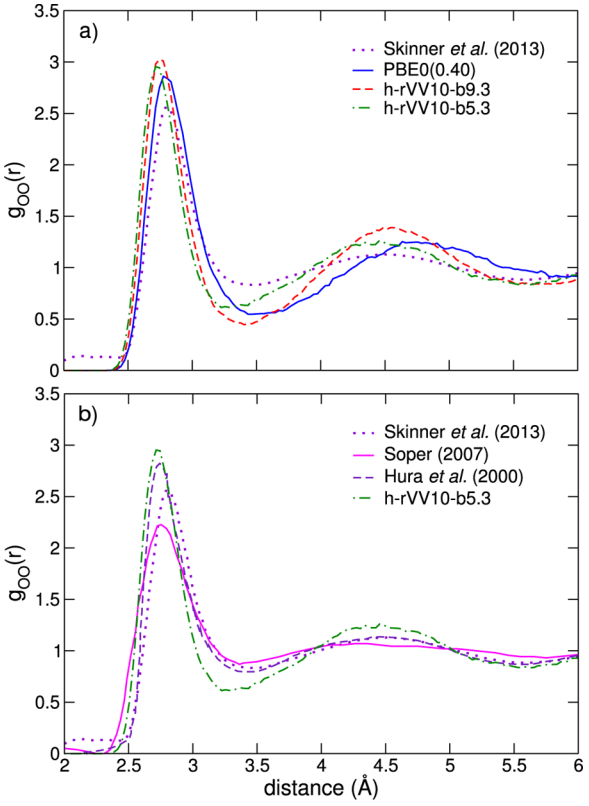

Figure 5. Oxygen−oxygen radial distribution functions as obtained with NpT MD simulations at 350 K compared to experimental results at ambient temperature (295−300 K). (a) Simulations based on PBE0(0.40), h-rVV10-b9.3, and h-rVV10-b5.3 compared with the experimental result from ref 107. (b) Simulation based on h-rVV10-b5.3 compared with various experimental results (refs 107−109).

While the results of Skinner et al.[107] are the most recent ones, it is instructive to compare our results with a larger set of experimental data, due to the uncertainty associated with different experiments (e.g., X-ray and neutron scattering).[110] In Figure 5b, we compare the oxygen−oxygen RDF obtained with h-rVV10-b5.3 with various experimental characterizations at ambient temperature (295−300 K),[107−109] which show sensible differences among them.[107−109] Despite these variations, it appears clearly that some degree of overstructuring is still present in the oxygen−oxygen RDF resulting from our simulation. As discussed above, these discrepancies are unlikely to be cured by the explicit consideration of nuclear quantum motions.[102]

From the previous section and from Figure 5, it is evident that, among the functionals studied here, h-rVV10-b5.3 provides the best description of the density and of the structural properties of liquid water. In Figure 6, we compare the corresponding oxygen−hydrogen and hydrogen−hydrogen RDFs with the experimental data at ambient temperature (298

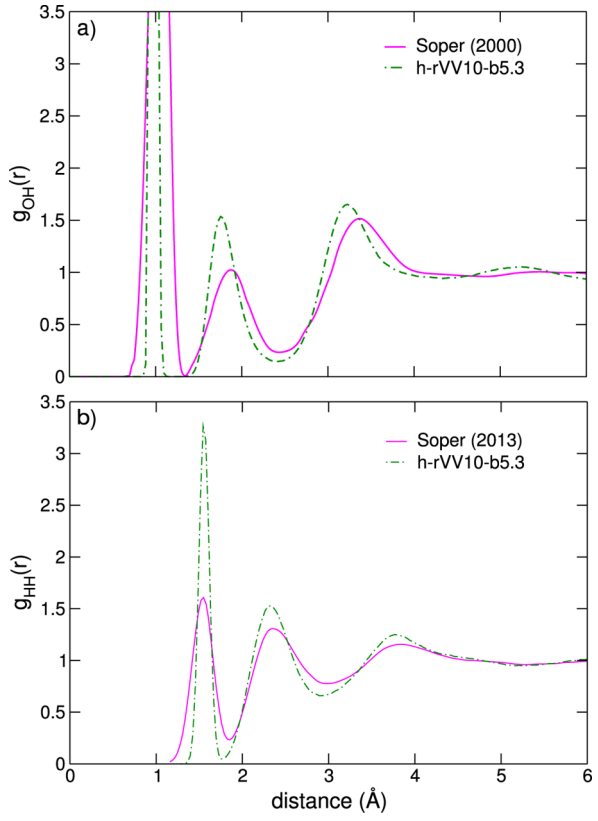

Figure 6. Oxygen−hydrogen (a) and hydrogen−hydrogen (b) radial distribution functions from NpT MD simulations at 350 K based on h-rVV10-b5.3, compared with the experimental data at ambient temperature (298 K) from refs 111 and 110.

DOI: 10.1021/acs.jpcb.6b03876
J. Phys. Chem. B 2016, 120, 7456−7470

K) from refs 111 and 110. The agreement with experiment achieved with h-rVV10-5.3 is overall good. In particular, it is comparable to that found for rVV10-b9.3 in ref 15. While recent path-integral simulations suggest that NQEs cannot completely correct the remaining discrepancies, their explicit treatment is nevertheless expected to slightly reduce the excess structure in the oxygen−hydrogen and hydrogen−hydrogen RDFs,[103] due to enhanced hydrogen-bond fluctuations.[50,101]

In conclusion, the RDFs at the h-rVV10 level are very similar to those obtained in ref 15 with the rVV10-b9.3 functional. This suggests that the optimization of the b parameter within the rVV10 scheme when combined with either a semilocal or a hybrid density functional yields the same qualitative improvement. Moreover, the obtained results are comparable to those achieved with other vdW schemes.[15,19,20,22,41] Although the level of agreement for the structural properties is not sensitively improved, we nevertheless find that the use of a hybrid functional yields a significantly improved description of the dynamical and electronic properties, as discussed in the following.

3.4. Hydrogen-Bond Network. A rough estimation of the hydrogen-bond network of liquid water is provided by the average number of hydrogen bonds, $\overline{n}_H$. This quantity, while not directly measurable, has been inferred from experiments at ambient conditions and amounts to 3.58.[112] The analysis of the hydrogen-bond network achieved with our MD simulations is performed providing a geometrical definition of the hydrogen bond, largely used in the literature:[15,49,112] a hydrogen bond between two molecules is identified when (i) the distance between two oxygen atoms is smaller than 3.5 Å and (ii) the O−H−O angle between the two water molecules is larger than 140°. Following this definition, we calculate $\overline{n}_H$ for all the simulations considered in our study (cf. Table 4).

Table 4. Average Percentage of Water Molecules Forming Three, Four, and Five Hydrogen Bonds and Average Number of Hydrogen Bonds, $\overline{n}_H$

	av percentage of water molecules (%)			
	3	4	5	$\overline{n}_H$
PBE0(0.40)	33	22	0	2.66
h-rVV10-b9.3	31	55	4	3.46
h-rVV10-b6.3	30	54	5	3.50
h-rVV10-b5.8	30	54	5	3.55
h-rVV10-b5.3	29	54	7	3.57
expt[112]				3.58

PBE0(0.40) gives $\overline{n}_H$ = 2.66, remarkably lower than the experimental estimate. This is connected to the low density achieved with PBE0(0.40), which results in a severely disrupted hydrogen-bond network. On average, 45% of the water molecules form two or fewer hydrogen bonds in this case (cf. Table 4). In contrast, we notice that when the functionals include nonlocal vdW interactions, the average number of hydrogen bonds differs by only ∼0.1 from the experimental estimate. The best agreement is achieved with h-rVV10-b5.3 ($\overline{n}_H$ = 3.57), which also yields an accurate value for the equilibrium mass density. Nevertheless, with the exception of PBE0(0.40), which suffers from a very weak hydrogen-bond strength, all other functionals yield close values, despite the large spread of equilibrium densities (0.87−1.02 g/cm^3). The present values for the average number of hydrogen bonds are also close to estimates in previous simulation studies.[15,16,22] These considerations call for a more sensitive descriptor of the hydrogen-bond network.

Therefore, we further analyze configurations with a given number of hydrogen bonds in terms of their total average coordination number, defined with same O−O cutoff distance (≲3.5 Å) employed for the definition of the hydrogen bond. In this way, it is possible to highlight sensible differences between different functionals. These are evident in the histogrammatic representation in Figure 7, where the fractions of water molecules forming a given number of hydrogen bonds are further decomposed into contributions from different coordinations. For PBE0(0.40), the structure is severely undercoordinated. At variance, the apparently similar hydrogen-bond networks obtained with h-rVV10-b9.3 and h-rVV10-5.3 show noticeably different coordinations. For the former, the 4-fold coordination is dominant and only a small fraction of higher

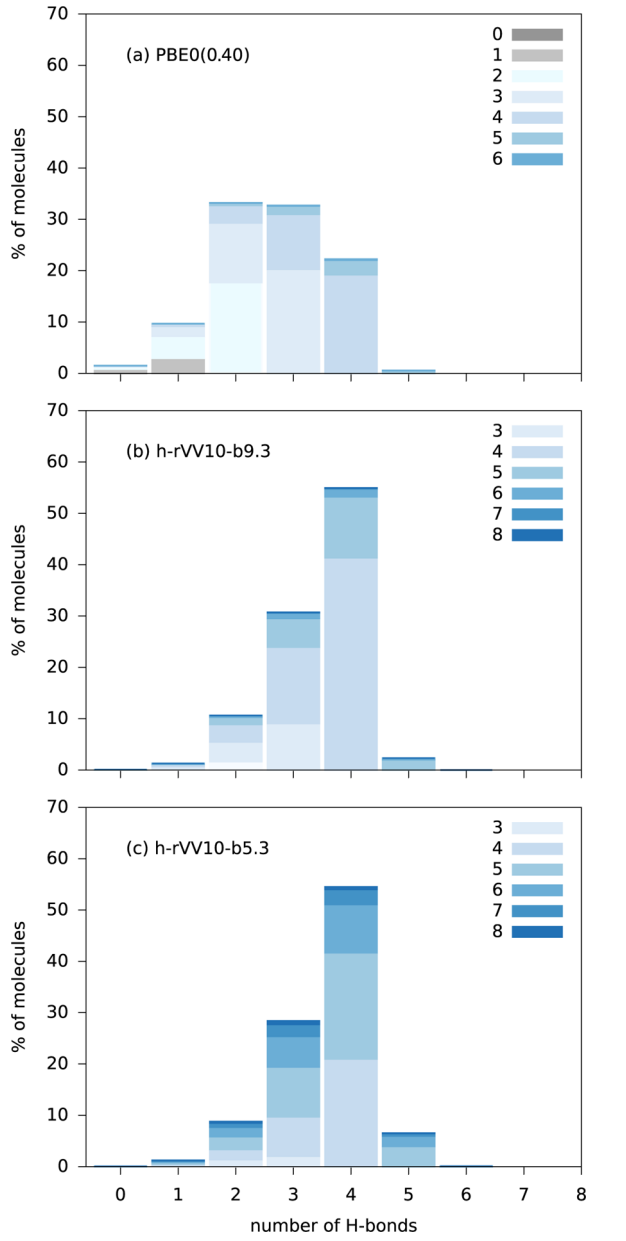

Figure 7. Distribution of coordination numbers pertaining to water molecules with a given number of hydrogen bonds.

DOI: 10.1021/acs.jpcb.6b03876
J. Phys. Chem. B 2016, 120, 7456−7470

coordinated molecules occur, recalling previous results obtained with PBE.[15] The latter shows a larger spread of coordinations, with an increased fraction of 5-fold coordinated water molecules (from ∼11% to ∼22%) and the appearance of noticeable fractions of 6-fold and 7-fold coordinated molecules.

For hybrid functionals, the change in density is subject to a delicate balance between directional bonding due to hydrogen-bond formation (cf. Table 1) and nondirectional bonding resulting from the nonlocal vdW interactions. The severe understructuring achieved with PBE0(0.40) is transformed into a PBE-like structure upon the inclusion of nonlocal vdW interactions with parameter b set to 9.3, likely resulting from the higher hydrogen-bond strength (cf. Table 1). As the parameter b is lowered to 5.3, the vdW interactions enforce a tighter packing and the system acquires the experimental density. The induced structural variations can be monitored by considering two descriptors of the local order. The first one concerns the O_c−O distances between the oxygen atom O_c of a central molecule and the O atoms belonging to first-neighbor water molecules. In Figure 8a, we show the distribution of such O_c−O distances distinguishing between contributions from the first four neighboring molecules and the fifth one, also known as the interstitial water molecule.[113] The analysis of the first coordination shell indicates that the position of the peak associated with the first four water molecules is only slightly affected as the water molecules get more packed. Nevertheless, for PBE0(0.40), we observe a noticeable shoulder at distances around 3.5 Å, which develops due to the occurrence of more distant third and fourth water molecules. The distribution of the fifth water molecule is sensibly shifted toward lower distances as higher coordinations are favored by vdW interactions. The vdW induced approach of the fifth molecule to the first coordination shell can be interpreted in analogy with the effect of pressure observed in experiments[114] and in simulations of liquid water.[113]

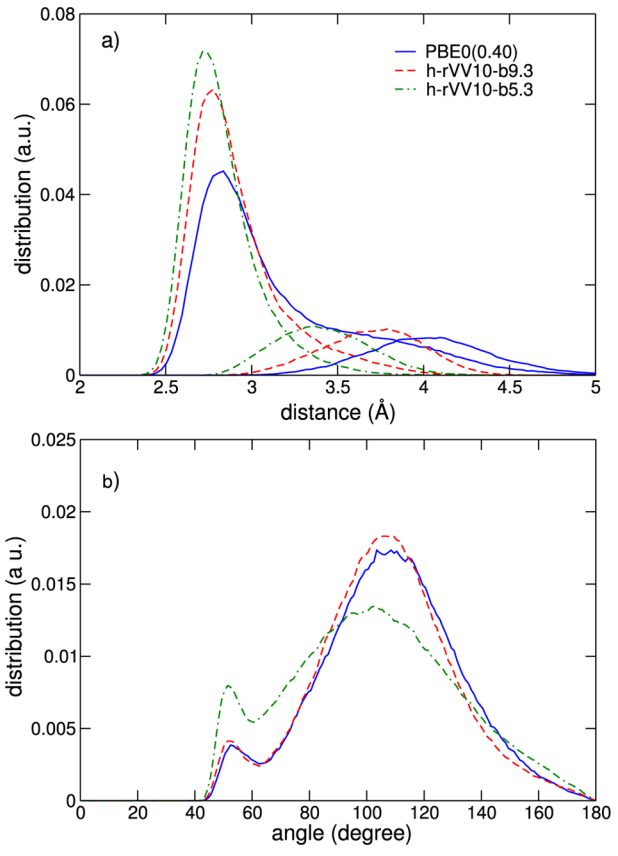

Figure 8. (a) Distribution of O_c−O distances between the central molecule and molecules in its first coordination shell, distinguishing the contributions from the first four neighbors and from the fifth one. (b) Distribution of the O−O_c−O angles associated with the central water molecule (O_c) and other two water molecules in the first coordination shell (O), defined by a cutoff of 3.5 Å for O_c−O separations.

The second descriptor relies on the O−O_c−O angles associated with the central water molecule (O_c) and other two water molecules in the first coordination shell (O), defined by a cutoff of 3.5 Å for O_c−O separations. Figure 8b shows the distribution of such angles. For PBE0(0.40), despite the low density that partially disrupts the hydrogen-bond network, an underlying tetrahedral order can still clearly be recognized in the O−O_c−O distribution. The shift of the principal peak away from 109° and the global broadening of the distribution denote the progressive weakening of the tetrahedral ordering as the vdW interactions increase.

3.5. Self-Diffusion Coefficient. We here study the performance of the adopted functionals in simulating the self-diffusion of water molecules. In order to isolate the effects of Fock exchange from those induced by vdW interactions, we perform NVE MD simulations at the experimental density with both PBE0(0.40) and h-rVV10-b5.3. We calculate the self-diffusion coefficient D from Einstein's relation, i.e., from the slope of the mean square displacement as a function of time. This quantity is evaluated as an average over all molecules. To estimate the error on diffusion coefficients obtained from 20 ps long trajectories, we perform a large set of independent MD simulations of this duration using an empirical potential but otherwise the same setup. The same percent error is then assumed to apply to the diffusion coefficients obtained from the hybrid functional MD simulations.

The evaluation of D is severely affected by finite-size effects. For a periodic supercell of size L = 12.42 Å, the underestimation with respect to the infinite-size limit can be quantified by[115,116]

$$\Delta D = \frac{k_B T \xi}{6\pi\eta L} \tag{2}$$

where k_B is the Boltzmann constant, ξ a constant value (2.84), and η the viscosity (3.12×10^{-4} Pa·s at T = 350 K, from ref 117). For our simulations based on 64-molecule supercells, ΔD = 1.9×10^5 cm^2/s. Since the experimental viscosity is employed in the determination of ΔD, we subtract this value from the experimental result, rather than adding it to the calculated values, following the approach used in ref 15.

D is also largely influenced by the temperature.[105] As experimental counterpart, we extrapolate the measured values from ref 105 to T = 350 K and obtain 6.2×10^{-5} cm^2/s. Accounting for the finite-size effects, we then derive the experimental reference of 4.3×10^{-5} cm^2/s (cf. Table 5), to which the diffusion constants from the simulations need to be compared.

Notwithstanding the uncertainty associated with the calculated values, the results listed in Table 5 indicate that both Fock exchange and vdW interactions have a beneficial effect on the calculated D. In fact, the inclusion of Fock exchange enhances the diffusion coefficient, as can be seen by

DOI: 10.1021/acs.jpcb.6b03876
J. Phys. Chem. B 2016, 120, 7456−7470

Table 5. Self-Diffusion Coefficient D as Achieved from NVE MD Simulation Based on PBE0(0.40) and h-rVV10-b5.3[a]

method	D (cm^2/s)
PBE0(0.40)	$(2.5 \pm 0.5) \times 10^{-5}$
h-rVV10-b5.3	$(3.2 \pm 0.6) \times 10^{-5}$
PBE[16,b]	0.47×10^{-5}
rVV10-b9.3[15]	1.5×10^{-5}
expt[105,115,116]	4.3×10^{-5}

[a]For comparison, we also report the experimental reference at $T = 350$ K[105] (see text for description) and calculated values from refs 15 and 16. [b]In ref 16, a 32-molecule supercell is used. In this case, the experimental reference for D is 3.8×10^{-5} cm^2/s.

comparing our PBE0(0.40) result with the PBE result from ref 16. The effect is large and leads to an enhancement of the diffusion coefficient by a factor of ∼5. This result supports observations from previous MD simulations at the hybrid functional level.[16] The beneficial effect of including Fock exchange can also be inferred by comparing h-rVV10-b5.3 with the rVV10-b9.3 result from ref 15.

The vdW interactions also contribute to enhancing the diffusion. In ref 15, it was found that the diffusion coefficient is enhanced by a factor of ∼3 when adding vdW interactions to a semilocal density functional. Here, we also find an enhancement of the diffusion coefficient when going from PBE0(0.40) to h-rVV10-b5.3. The combined effect of Fock exchange and vdW interactions results in a value of $D = (3.2 \pm 0.6) \times 10^{-5}$ cm^2/s, which compares very favorably with the experimental reference set at 4.3×10^{-5} cm^2/s.

3.6. Electronic Structure. We obtain the conduction and valence band edges by extrapolation of the wing of the respective near-edge density of states (DOS). The separation between the band edges obtained in this way defines the electronic band gap E_g of liquid water. This way of extracting the band gap is analogous to the experimental procedure[56,57] and carries the additional advantage of being robust against finite-size effects.[49] The inclusion of vdW interactions in the functional has been shown to affect the band gap by only ∼0.1 eV when averaged over a given set of MD configurations.[49] However, when the structural configurations are taken from a MD simulation obtained consistently with the adopted functional, the vdW interactions directly determine the equilibrium density and the calculated band gap is found to be sensibly affected. Figure 9 illustrates the dependence of the calculated E_g on the equilibrium density. As the parameter b decreases and the structures become more compact, the band gap is found to decrease. The observed trend is given by the balance between (i) an increase in the band gap induced by a higher density [this is evident when MD simulations at different fixed densities are performed at the same level of theory; PBE0(0.40) in Figure 9, consistent with the results in ref 118] and (ii) a decrease in the band gap induced by the increase of the extent of nonlocal vdW interactions, controlled by the b parameter in the rVV10 scheme.

From the NpT simulations performed with PBE0 and h-rVV10-b9.3, we obtain band gaps of 8.9 and 8.8 eV, which overestimate the experimental estimate of 8.7 eV (ref 53) by ∼0.2 and ∼0.1 eV, respectively. For the h-rVV10-b5.3 functional, the density approaches the experimental value and we obtain $E_g = 8.75$ eV, in agreement with experiment within 0.1 eV. The difference in band gap induced by the use of different functionals can be quantified. As can be seen in Figure 9, the band gap decreases as the b parameter is set to lower values, the difference with the PBE0(0.40) band gap being ∼0.2 eV for h-rVV10-b9.3 at a density of 0.87 g/cm^3, and ∼0.30 eV for h-rVV10-b5.3 at 1.02 g/cm^3. These values include both the structural effect and the effect of using different functionals. The size of these two contributions can be separately identified from the calculation of the band gap at the PBE0(0.40) level on structural configurations achieved at the h-rVV10-b5.3 level and vice versa. We find that the decrease of 0.3 eV going from PBE0(0.40) to h-rVV10-b5.3 is mainly due to the use of a different functional (0.2 eV), while the structural effect is modest (<0.1 eV), as already observed in ref 49.

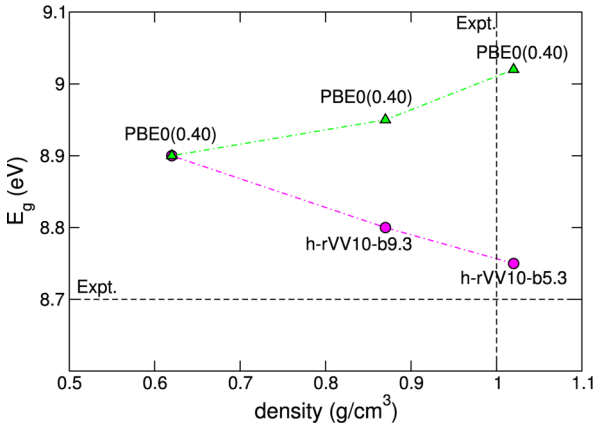

Figure 9. Electronic band gap (E_g) of liquid water as a function of the equilibrium density obtained with various functionals and with the same functional [PBE0(0.40)] at different fixed densities.

Next, we investigate the absolute positions of the band edges. This requires the determination of a physical reference, for which we take the standard hydrogen electrode (SHE). To determine the SHE level relative to band structure achieved with the PBE0(0.40) and h-rVV10-b5.3 functionals, we rely on a computational version of the SHE.[47,49,119] The redox level defining the SHE is calculated within a formulation which gives a grand-canonical description of the number of electrons in the system.[49,120] In this formulation, the free energy of a solute $G_f^q[X]$ is expressed as a function of the electron chemical potential μ:

$$G_f^q[\mathrm{X}] = G^q[\mathrm{X}] - G[\mathrm{bulk}] - \sum_i n_i\mu_i + q(\varepsilon_v + \mu) + E_{corr}^q \quad (3)$$

where $G^q[X]$ is the free energy of the solute X in the charge state q, $E[\mathrm{bulk}]$ is the free energy of the pristine bulk system (liquid water), μ_i is the chemical potential of the subtracted/added species i, ε_v is the VBM of the pristine system, and E_{corr}^q is a finite-size correction.

The finite-size correction is obtained through the Freysoldt–Neugebauer–Van de Walle (FNV) scheme.[121,122] In this scheme, the spurious electrostatic effects are corrected considering two energy contributions: (i) the Madelung energy, which accounts for the spurious interactions due to the use of periodic boundary conditions (PBC), and (ii) an alignment-like term which results from the finite extent of the charge distribution of the solute. The former term is found to be very small (0.03 eV), due to the high dielectric constant (78.3) of water at ambient temperature and atmospheric pressure. The latter term can be evaluated from the shift of the average electrostatic potential in a region far from the solute with respect to the pristine bulk system. In practice, we estimate this

DOI: 10.1021/acs.jpcb.6b03876
J. Phys. Chem. B 2016, 120, 7456–7470

contribution from the shift of the O 2s peak and find it to be negligible in our case.

In analogy to the study of charge transition levels in crystalline materials,[122,123] we then define the redox level $\mu(q/q')$ as the electron chemical potential for which the free energies of formation of a solute X in the charge states q and q' are equal, $\Delta G(q/q') = 0$.[49] This results in the following expression for $\mu(q/q')$:

$$\mu(q/q') = \frac{G^q[\mathrm{X}] - G^{q'}[\mathrm{X}]}{q' - q} + \frac{E^q_{\mathrm{corr}} - E^{q'}_{\mathrm{corr}}}{q' - q} - \varepsilon_{\mathrm{v}} \quad (4)$$

We evaluate the free-energy differences appearing in eq 4 by combining the thermodynamic integration (TI) method with DFT-MD simulations.[124,125] We thus define a fictitious Hamiltonian $\mathcal{H}_\eta$,

$$\mathcal{H}_\eta = (1 - \eta)\mathcal{H}_{\mathrm{R}} + \eta\mathcal{H}_{\mathrm{P}} \quad (5)$$

which connects the Hamiltonians of the reactant, $\mathcal{H}_{\mathrm{R}}$, and of the product, $\mathcal{H}_{\mathrm{P}}$, via the Kirkwood coupling parameter $0 \le \eta \le 1$.[124,125] As variations of volumes are negligible for small solutes, we actually consider the Helmholtz free energy.[49] It is demonstrated that the variation in the free energy ΔA associated with the R → P reaction can be expressed as the integral of the average vertical energy gap between P and R over the interval of variation of η:[124,125]

$$\Delta A = \int_0^1 \langle E \rangle_\eta \, \mathrm{d}\eta \quad (6)$$

For the SHE, we adopt the following half-reaction:

$$\mathrm{H_3O^+(aq)} + \mathrm{e^-} = \mathrm{H_2O(l)} + \frac{1}{2}\mathrm{H_2(g)} \quad (7)$$

for which the redox level referred to the valence band of liquid water can be expressed as follows:[49]

$$\mu(\mathrm{SHE}) = \Delta_{\mathrm{dp}}A_{\mathrm{H_3O^+}} - \Delta_{\mathrm{zp}}E_{\mathrm{H_3O^+}} + \mu_{\mathrm{H}} - \varepsilon_{\mathrm{v}} - E^{q=+1}_{\mathrm{corr}} \quad (8)$$

where $\Delta_{\mathrm{dp}}A_{\mathrm{H_3O^+}}$ is the integral associated with the deprotonation reaction of the hydronium cation. $\Delta_{\mathrm{zp}}E_{\mathrm{H_3O^+}}$ is a correction to $\Delta_{\mathrm{dp}}A_{\mathrm{H_3O^+}}$, which accounts for the lack of nuclear quantum motions in our MD simulations. It is evaluated from the peak frequencies in the experimental vibrational spectrum of the hydrated proton.[126] μ_{H} is the chemical potential of hydrogen and includes rotational, translational, and vibrational free energy contributions in standard conditions (T = 298 K and concentration of 1 mol/L).[49] The calculated value of μ_{H} is reported in Table 6, along with the free energy of formation of the proton in the gas phase $\Delta_{\mathrm{f}}G^{\mathrm{g},0}_{\mathrm{H^+}} = \mu_{\mathrm{H^+}} - \mu_{\mathrm{H}}$ = 15.60 eV, to be compared with the experimental estimate of 15.81 eV.[127]

In this work, we perform MD simulations of the hydronium cation based on PBE0(0.40) and h-rVV10-b5.3, using the same computational setup as described in ref 49. For three different values of η, we obtain the vertical deprotonation energies $\Delta_{\mathrm{dp}}E_{\mathrm{H_3O^+}}$ through averages over the MD trajectory. The calculated values for $\Delta_{\mathrm{dp}}E_{\mathrm{H_3O^+}}$ are reported in Figure 10 for PBE0(0.40) and h-rVV10-b5.3. The figure also reports results obtained in ref 49 with PBE0(0.40) on structural configurations from molecular dynamics based on rVV10-b9.3 and PBE. The present results obtained with h-rVV10-b5.3 are close to the non-self-consistent results of ref 49, showing differences smaller than 0.1 and 0.25 eV, respectively. From this comparison, we infer that vdW interactions have a modest effect on the deprotonation energies of H_3O^+. Through the thermodynamic integration of the deprotonation energies in Figure 10, we then obtain the associated free-energy difference:

$$\Delta_{\mathrm{dp}}A_{\mathrm{H_3O^+}} = \int_0^1 \langle \Delta_{\mathrm{dp}}E_{\mathrm{H_3O^+}} \rangle_\eta \, \mathrm{d}\eta \quad (9)$$

The calculated value of $\Delta_{\mathrm{dp}}A_{\mathrm{H_3O^+}}$ referred to the hydrogen chemical potential and aligned with respect to the VBM of water is reported in Table 6.

Equation 8 allows us to position the VBM and the CBM with respect to the SHE level (cf. Figure 11). While retaining the same accuracy in the description of the VBM found in ref 49, where the same functional was used on structural configurations at the PBE and rVV10 levels, self-consistent PBE0(0.40) results show a worsened agreement in the description of the CBM, which is shifted 0.3 eV away from the experiment. Our h-rVV10-b5.3 calculated values are in very good agreement with recent measurements,[48,53,56−58] showing differences smaller than 0.1 eV. This result slightly improves upon the agreement in ref 49, where the calculations were performed at the PBE0(0.40) level on structural configuration achieved at the rVV10 level of theory. In particular, the agreement with experiment is improved by 0.1 eV for the VBM and by 0.2 eV for the CBM (cf. Figure 11). These small differences confirm the weak correlation between the structural

Table 6. Valence-Band and Conduction-Band Edges of Liquid Water Calculated with h-rVV10-b5.3 and Referred to the SHE Level[a]

	theory	expt
VBM	4.84	4.9[48,56,57]
CBM	−3.91	−3.9[58]
$\Delta_{\mathrm{dp}}A_{\mathrm{H_3O^+}} + \mu_{\mathrm{H}} - \varepsilon_{\mathrm{v}}$	5.22	
$\Delta_{\mathrm{zp}}E_{\mathrm{H_3O^+}}$		0.36[126]
μ_{H}	−15.79	
$\mu_{\mathrm{H^+}}$	−0.19	
$\Delta_{\mathrm{f}}G^{\mathrm{g},0}_{\mathrm{H^+}}$	15.60	15.81[127]
$E^{q=+1}_{\mathrm{corr}}$	0.03	

[a]We also give various quantities required for the evaluation of the SHE level: $\Delta_{\mathrm{dp}}A_{\mathrm{H_3O^+}}$, μ_{H}, $\mu_{\mathrm{H^+}}$, $\Delta_{\mathrm{f}}G^{\mathrm{g},0}_{\mathrm{H^+}}$, and $E^{q=+1}_{\mathrm{corr}}$. When available, experimental values are also reported. All energies are in eV.

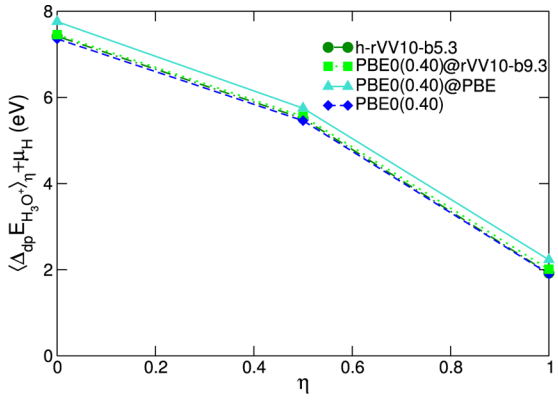

Figure 10. Average vertical energy gaps of deprotonation, $\langle \Delta_{\mathrm{dp}}E_{\mathrm{H_3O^+}} \rangle_\eta$. The energies are referred to the VBM of liquid water as obtained with h-rVV10-b5.3.

DOI: 10.1021/acs.jpcb.6b03876
J. Phys. Chem. B 2016, 120, 7456−7470

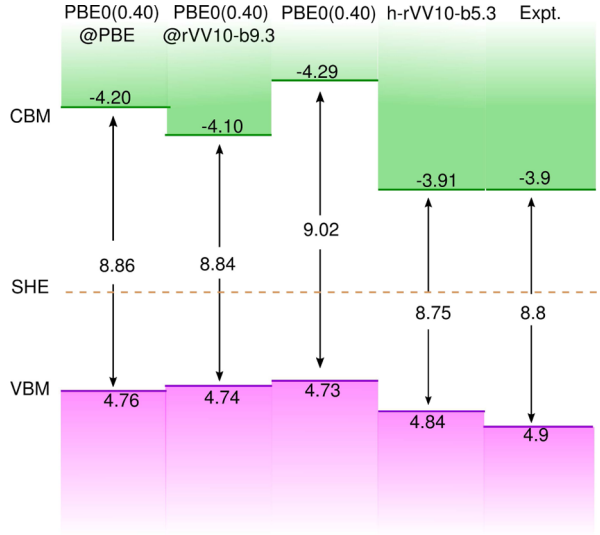

Figure 11. Conduction-band and valence-band edges (eV) of liquid water calculated with h-rVV10-b5.3 and PBE0(0.40), compared to experimental data from refs 48 and 56−58 and previous theoretical results from ref 49, where calculations where performed with PBE0(0.40) on structural configurations achieved at the PBE and rVV10-b9.3 levels. The band edges are referred to the SHE level. Energies are in eV.

and the electronic properties of liquid water, already remarked in ref 49.

4. CONCLUSIONS

We reported the results obtained from a study of the structural, dynamical, and electronic properties of liquid water, achieved at the hybrid functional level of theory. We employed a hybrid functional within the PBE0 formalism with a fraction of Fock exchange set to α = 0.40 and included the effect of vdW interactions through a nonlocal functional. We first tested the performance of this approach for the hydrogen-bond energy of the water dimer, the stability of water hexamer clusters, and the physical properties of ice I_h and VIII. We found that the inclusion of vdW interactions in the hybrid functional compensates its tendency of producing weaker hydrogen bonds than semilocal density functionals. Moreover, from the analysis of the relative stability of extended and compact structural motifs in water clusters (prism-shaped and ring-shaped hexamers) and in solid state water (ice I_h and VIII), we observe that the latter are correctly described by theory only when vdW interactions are accounted for. From the analysis of the equilibrium mass density, the hydrogen-bond network, and the local-order parameters achieved with MD simulations in the NpT statistical ensemble, we found that liquid water is severely understructured when described with a hybrid functional which does not account for vdW interactions. This is a consequence of the combination of two shortcomings of the hybrid functional: (i) the low hydrogen-bond energy and (b) the low stability of compact structural configurations. Therefore, we supplemented the hybrid functional with the nonlocal VV10 scheme and optimized its empirical parameter b to reproduce the experimental density. The functional obtained in this way was then examined against its ability in describing the structural, dynamical, and electronic properties of liquid water. As far as the radial distribution functions are concerned, no significant improvement is recorded with respect to those achieved with the nonhybrid rVV10-b9.3. In contrast, the self-diffusion coefficient is shown to improve noticeably, due to the combination of Fock exchange and vdW interactions, which both contribute in bringing the calculated values closer to the experimental estimate. The electronic properties are also calculated and found to be in excellent agreement with recent photoemission spectroscopy and solvent polarization studies. In particular, both the band gap and the band edges are found to deviate by less than 0.1 eV from their experimental counterparts.

In conclusion, the employed functional including both Fock exchange and nonlocal vdW interactions allows for a simultaneous description of the structural, dynamical, and electronic properties of liquid water in overall good agreement with experiment. Therefore, this description is expected to be suitable for the study of redox levels, particularly when they lie near the band edges, and in applications where the correction of the self-interaction error is fundamental to achieve a physical MD trajectory, for instance in the description of solvated electrons and holes.

AUTHOR INFORMATION

Corresponding Author

*E-mail: Francesco.Ambrosio@epfl.ch. Phone: +41 21 6933423. Fax: +41 21 693 5419.

Notes

The authors declare no competing financial interest.

ACKNOWLEDGMENTS

We thank Julia Wiktor for useful discussions. This work has been performed in the context of the National Center of Competence in Research (NCCR): Materials' Revolution: Computational Design and Discovery of Novel Materials (MARVEL) of the Swiss National Science Foundation. We used computational resources of CSCS and CSEA-EPFL.

REFERENCES

(1) Ball, P. Water: Water - an enduring mystery. *Nature* **2008**, *452*, 291−292.
(2) Ball, P. *Astrochemistry and Astrobiology*; Springer-Verlag: Berlin Heidelberg, 2013; pp 169−210.
(3) Nilsson, A.; Pettersson, L. G. M. The structural origin of anomalous properties of liquid water. *Nat. Commun.* **2015**, *6*, 8998.
(4) Gillan, M. J.; Alfè, D.; Michaelides, A. Perspective: How good is DFT for water? *J. Chem. Phys.* **2016**, *144*, 130901.
(5) Jorgensen, W. L.; Chandrasekhar, J.; Madura, J. D.; Impey, R. W.; Klein, M. L. Comparison of simple potential functions for simulating liquid water. *J. Chem. Phys.* **1983**, *79*, 926−935.
(6) Mahoney, M. W.; Jorgensen, W. L. A five-site model for liquid water and the reproduction of the density anomaly by rigid, nonpolarizable potential functions. *J. Chem. Phys.* **2000**, *112*, 8910−8922.
(7) Laasonen, K.; Sprik, M.; Parrinello, M.; Car, R. *Ab initio* liquid water. *J. Chem. Phys.* **1993**, *99*, 9080−9089.
(8) Sprik, M.; Hutter, J.; Parrinello, M. *Ab initio* molecular dynamics simulation of liquid water: Comparison of three gradient-corrected density functionals. *J. Chem. Phys.* **1996**, *105*, 1142−1152.
(9) Izvekov, S.; Voth, G. A. Car-Parrinello molecular dynamics simulation of liquid water: new results. *J. Chem. Phys.* **2002**, *116*, 10372−10376.
(10) Grossman, J. C.; Schwegler, E.; Draeger, E. W.; Gygi, F.; Galli, G. Towards an assessment of the accuracy of density functional theory for first principles simulations of water. *J. Chem. Phys.* **2004**, *120*, 300−311.

DOI: 10.1021/acs.jpcb.6b03876
J. Phys. Chem. B 2016, 120, 7456−7470

(11) VandeVondele, J.; Mohamed, F.; Krack, M.; Hutter, J.; Sprik, M.; Parrinello, M. The influence of temperature and density functional models in *ab initio* molecular dynamics simulation of liquid water. *J. Chem. Phys.* **2005**, *122*, 014515.
(12) Sit, P. H.-L.; Marzari, N. Static and dynamical properties of heavy water at ambient conditions from first-principles molecular dynamics. *J. Chem. Phys.* **2005**, *122*, 204510.
(13) Lee, H.-S.; Tuckerman, M. E. Dynamical properties of liquid water from *ab initio* molecular dynamics performed in the complete basis set limit. *J. Chem. Phys.* **2007**, *126*, 164501.
(14) Schmidt, J.; VandeVondele, J.; Kuo, I.-F. W.; Sebastiani, D.; Siepmann, J. I.; Hutter, J.; Mundy, C. J. Isobaric-isothermal molecular dynamics simulations utilizing density functional theory: an assessment of the structure and density of water at near-ambient conditions. *J. Phys. Chem. B* **2009**, *113*, 11959−11964.
(15) Miceli, G.; de Gironcoli, S.; Pasquarello, A. Isobaric first-principles molecular dynamics of liquid water with nonlocal van der Waals interactions. *J. Chem. Phys.* **2015**, *142*, 034501.
(16) Todorova, T.; Seitsonen, A. P.; Hutter, J.; Kuo, I.-F. W.; Mundy, C. J. Molecular dynamics simulation of liquid water: hybrid density functionals. *J. Phys. Chem. B* **2006**, *110*, 3685−3691.
(17) Guidon, M.; Schiffmann, F.; Hutter, J.; VandeVondele, J. *Ab initio* molecular dynamics using hybrid density functionals. *J. Chem. Phys.* **2008**, *128*, 214104.
(18) Guidon, M.; Hutter, J.; VandeVondele, J. Auxiliary density matrix methods for Hartree-Fock exchange calculations. *J. Chem. Theory Comput.* **2010**, *6*, 2348−2364.
(19) Del Ben, M.; Hutter, J.; VandeVondele, J. Probing the structural and dynamical properties of liquid water with models including non-local electron correlation. *J. Chem. Phys.* **2015**, *143*, 054506.
(20) DiStasio, R. A.; Santra, B.; Li, Z.; Wu, X.; Car, R. The individual and collective effects of exact exchange and dispersion interactions on the *ab initio* structure of liquid water. *J. Chem. Phys.* **2014**, *141*, 084502.
(21) Santra, B.; DiStasio, R. A.; Martelli, F.; Car, R. Local structure analysis in *ab initio* liquid water. *Mol. Phys.* **2015**, *113*, 2829−2841.
(22) Gaiduk, A. P.; Gygi, F.; Galli, G. Density and compressibility of liquid water and ice from first-principles simulations with hybrid functionals. *J. Phys. Chem. Lett.* **2015**, *6*, 2902−2908.
(23) Perdew, J. P.; Ernzerhof, M.; Burke, K. Rationale for mixing exact exchange with density functional approximations. *J. Chem. Phys.* **1996**, *105*, 9982−9985.
(24) Adamo, C.; Barone, V. Toward reliable density functional methods without adjustable parameters: the PBE0 model. *J. Chem. Phys.* **1999**, *110*, 6158−6170.
(25) Becke, A. D. Density-functional thermochemistry. III. The role of exact exchange. *J. Chem. Phys.* **1993**, *98*, 5648−5652.
(26) Xu, X.; Goddard, W. A. The X3LYP extended density functional for accurate descriptions of nonbond interactions, spin states, and thermochemical properties. *Proc. Natl. Acad. Sci. U. S. A.* **2004**, *101*, 2673−2677.
(27) Perdew, J. P.; Burke, K.; Ernzerhof, M. Generalized gradient approximation made simple. *Phys. Rev. Lett.* **1996**, *77*, 3865−3868.
(28) Heyd, J.; Scuseria, G. E.; Ernzerhof, M. Hybrid functionals based on a screened Coulomb potential. *J. Chem. Phys.* **2003**, *118*, 8207−8215.
(29) Lippert, G.; Hutter, J.; Parrinello, M. The Gaussian and augmented-plane-wave density functional method for *ab initio* molecular dynamics simulations. *Theor. Chem. Acc.* **1999**, *103*, 124−140.
(30) VandeVondele, J.; Krack, M.; Mohamed, F.; Parrinello, M.; Chassaing, T.; Hutter, J. Quickstep: Fast and accurate density functional calculations using a mixed Gaussian and plane waves approach. *Comput. Phys. Commun.* **2005**, *167*, 103−128.
(31) Car, R.; Parrinello, M. Unified approach for molecular dynamics and density-functional theory. *Phys. Rev. Lett.* **1985**, *55*, 2471−2474.
(32) Wu, X.; Selloni, A.; Car, R. Order-*N* implementation of exact exchange in extended insulating systems. *Phys. Rev. B: Condens. Matter Mater. Phys.* **2009**, *79*, 085102.
(33) Grimme, S. Accurate description of van der Waals complexes by density functional theory including empirical corrections. *J. Comput. Chem.* **2004**, *25*, 1463−1473.
(34) Dion, M.; Rydberg, H.; Schröder, E.; Langreth, D. C.; Lundqvist, B. I. Van der Waals density functional for general geometries. *Phys. Rev. Lett.* **2004**, *92*, 246401.
(35) Dion, M.; Rydberg, H.; Schröder, E.; Langreth, D. C.; Lundqvist, B. I. Erratum: van der Waals density functional for general geometries [Phys. Rev. Lett. **92**, 246401 (2004)]. *Phys. Rev. Lett.* **2005**, *95*, 109902.
(36) Thonhauser, T.; Cooper, V. R.; Li, S.; Puzder, A.; Hyldgaard, P.; Langreth, D. C. Van der Waals density functional: Self-consistent potential and the nature of the van der Waals bond. *Phys. Rev. B: Condens. Matter Mater. Phys.* **2007**, *76*, 125112.
(37) Tkatchenko, A.; Scheffler, M. Accurate molecular van Der Waals interactions from ground-state electron density and free-atom reference data. *Phys. Rev. Lett.* **2009**, *102*, 073005.
(38) Lee, K.; Murray, E. D.; Kong, L.; Lundqvist, B. I.; Langreth, D. C. Higher-accuracy van der Waals density functional. *Phys. Rev. B: Condens. Matter Mater. Phys.* **2010**, *82*, 081101.
(39) Cooper, V. R. Van der Waals density functional: An appropriate exchange functional. *Phys. Rev. B: Condens. Matter Mater. Phys.* **2010**, *81*, 161104.
(40) Vydrov, O. A.; Van Voorhis, T. Nonlocal van der Waals density functional: The simpler the better. *J. Chem. Phys.* **2010**, *133*, 244103.
(41) Murdachaew, G.; Mundy, C. J.; Schenter, G. K. Improving the density functional theory description of water with self-consistent polarization. *J. Chem. Phys.* **2010**, *132*, 164102.
(42) Møller, C.; Plesset, M. S. Note on an approximation treatment for many-electron systems. *Phys. Rev.* **1934**, *46*, 618−622.
(43) Head-Gordon, M.; Pople, J. A.; Frisch, M. J. MP2 energy evaluation by direct methods. *Chem. Phys. Lett.* **1988**, *153*, 503−506.
(44) Ren, X.; Rinke, P.; Joas, C.; Scheffler, M. Random-phase approximation and its applications in computational chemistry and materials science. *J. Mater. Sci.* **2012**, *47*, 7447−7471.
(45) Sabatini, R.; Gorni, T.; de Gironcoli, S. Nonlocal van der Waals density functional made simple and efficient. *Phys. Rev. B: Condens. Matter Mater. Phys.* **2013**, *87*, 041108.
(46) Adriaanse, C.; Cheng, J.; Chau, V.; Sulpizi, M.; VandeVondele, J.; Sprik, M. Aqueous redox chemistry and the electronic band structure of liquid water. *J. Phys. Chem. Lett.* **2012**, *3*, 3411−3415.
(47) Cheng, J.; Sprik, M. Alignment of electronic energy levels at electrochemical interfaces. *Phys. Chem. Chem. Phys.* **2012**, *14*, 11245−11267.
(48) Pham, T. A.; Zhang, C.; Schwegler, E.; Galli, G. Probing the electronic structure of liquid water with many-body perturbation theory. *Phys. Rev. B: Condens. Matter Mater. Phys.* **2014**, *89*, 060202.
(49) Ambrosio, F.; Miceli, G.; Pasquarello, A. Redox levels in aqueous solution: effect of van der Waals interactions and hybrid functionals. *J. Chem. Phys.* **2015**, *143*, 244508.
(50) Chen, W.; Ambrosio, F.; Miceli, G.; Pasquarello, A. *Ab initio* electronic structure of liquid water. Submitted.
(51) Cohen, A. J.; Mori-Sánchez, P.; Yang, W. Challenges for density functional theory. *Chem. Rev.* **2012**, *112*, 289−320.
(52) Marsman, M.; Paier, J.; Stroppa, A.; Kresse, G. Hybrid functionals applied to extended systems. *J. Phys.: Condens. Matter* **2008**, *20*, 064201.
(53) Bernas, A.; Ferradini, C.; Jay-Gerin, J.-P. On the electronic structure of liquid water: Facts and reflections. *Chem. Phys.* **1997**, *222*, 151−160.
(54) Lee, C.; Yang, W.; Parr, R. G. Development of the Colle-Salvetti correlation-energy formula into a functional of the electron density. *Phys. Rev. B: Condens. Matter Mater. Phys.* **1988**, *37*, 785−789.
(55) Becke, A. D. Density-functional exchange-energy approximation with correct asymptotic behavior. *Phys. Rev. A: At., Mol., Opt. Phys.* **1988**, *38*, 3098−3100.
(56) Winter, B.; Faubel, M.; Hertel, I. V.; Pettenkofer, C.; Bradforth, S. E.; Jagoda-Cwiklik, B.; Cwiklik, L.; Jungwirth, P. Electronic binding energies of hydrated $H3O^+$ and OH^-: photoelectron spectroscopy of

DOI: 10.1021/acs.jpcb.6b03876
J. Phys. Chem. B 2016, 120, 7456−7470

aqueous acid and base solutions combined with electronic structure calculations. *J. Am. Chem. Soc.* **2006**, *128*, 3864−3865.
(57) Seidel, R.; Thürmer, S.; Winter, B. Photoelectron spectroscopy meets aqueous solution: studies from a vacuum liquid microjet. *J. Phys. Chem. Lett.* **2011**, *2*, 633−641.
(58) Coe, J. V.; Earhart, A. D.; Cohen, M. H.; Hoffman, G. J.; Sarkas, H. W.; Bowen, K. H. Using cluster studies to approach the electronic structure of bulk water: Reassessing the vacuum level, conduction band edge, and band gap of water. *J. Chem. Phys.* **1997**, *107*, 6023−6031.
(59) Chen, W.; Pasquarello, A. Accurate band gaps of extended systems via efficient vertex corrections in GW. *Phys. Rev. B: Condens. Matter Mater. Phys.* **2015**, *92*, 041115.
(60) Sharma, S.; Dewhurst, J. K.; Sanna, A.; Gross, E. K. U. Bootstrap approximation for the exchange-correlation kernel of time-dependent density-functional theory. *Phys. Rev. Lett.* **2011**, *107*, 186401.
(61) Habershon, S.; Manolopoulos, D. E.; Markland, T. E.; Miller, T. F., III Ring-polymer molecular dynamics: quantum effects in chemical dynamics from classical trajectories in an extended phase space. *Annu. Rev. Phys. Chem.* **2013**, *64*, 387−413.
(62) Ma, J.; Schmidhammer, U.; Pernot, P.; Mostafavi, M. Reactivity of the strongest oxidizing species in aqueous Solutions: the short-lived radical cation $H_2O^{+\cdot}$. *J. Phys. Chem. Lett.* **2014**, *5*, 258−261.
(63) Turi, L.; Rossky, P. J. Theoretical studies of spectroscopy and dynamics of hydrated electrons. *Chem. Rev.* **2012**, *112*, 5641−5674.
(64) Schwarz, H. A. Free radicals generated by radiolysis of aqueous solutions. *J. Chem. Educ.* **1981**, *58*, 101.
(65) Marsalek, O.; Elles, C. G.; Pieniazek, P. A.; Pluharova, E.; VandeVondele, J.; Bradforth, S. E.; Jungwirth, P. Chasing charge localization and chemical reactivity following photoionization in liquid water. *J. Chem. Phys.* **2011**, *135*, 224510.
(66) Grimme, S.; Antony, J.; Ehrlich, S.; Krieg, H. A consistent and accurate *ab initio* parametrization of density functional dispersion correction (DFT-D) for the 94 elements H-Pu. *J. Chem. Phys.* **2010**, *132*, 154104.
(67) Goerigk, L.; Grimme, S. A thorough benchmark of density functional methods for general main group thermochemistry, kinetics, and noncovalent interactions. *Phys. Chem. Chem. Phys.* **2011**, *13*, 6670−6688.
(68) Komsa, H.-P.; Broqvist, P.; Pasquarello, A. Alignment of defect levels and band edges through hybrid functionals: Effect of screening in the exchange term. *Phys. Rev. B: Condens. Matter Mater. Phys.* **2010**, *81*, 205118.
(69) Chen, W.; Pasquarello, A. Band-edge positions in GW: effects of starting point and self-consistency. *Phys. Rev. B: Condens. Matter Mater. Phys.* **2014**, *90*, 165133.
(70) Dunning, T. H. Gaussian basis sets for use in correlated molecular calculations. I. The atoms boron through neon and hydrogen. *J. Chem. Phys.* **1989**, *90*, 1007−1023.
(71) Miceli, G.; Hutter, J.; Pasquarello, A. Liquid water through density-functional molecular dynamics: plane-wave vs. atomic-orbital basis sets. *J. Chem. Theory Comput.* **2016**, accepted DOI: 10.1021/acs.jctc.6b00271.
(72) Giannozzi, P.; Baroni, S.; Bonini, N.; Calandra, M.; Car, R.; Cavazzoni, C.; Ceresoli, D.; Chiarotti, G. L.; Cococcioni, M.; Dabo, I.; et al. QUANTUM ESPRESSO: a modular and open-source software project for quantum simulations of materials. *J. Phys.: Condens. Matter* **2009**, *21*, 395502.
(73) Goedecker, S.; Teter, M.; Hutter, J. Separable dual-space Gaussian pseudopotentials. *Phys. Rev. B: Condens. Matter Mater. Phys.* **1996**, *54*, 1703−1710.
(74) Hartwigsen, C.; Goedecker, S.; Hutter, J. Relativistic separable dual-space Gaussian pseudopotentials from H to Rn. *Phys. Rev. B: Condens. Matter Mater. Phys.* **1998**, *58*, 3641−3662.
(75) Guidon, M.; Hutter, J.; VandeVondele, J. Robust periodic Hartree-Fock exchange for large-scale simulations using Gaussian basis sets. *J. Chem. Theory Comput.* **2009**, *5*, 3010−3021.
(76) Guidon, M.; Hutter, J.; VandeVondele, J. Auxiliary density matrix methods for Hartree-Fock exchange calculations. *J. Chem. Theory Comput.* **2010**, *6*, 2348−2364.
(77) Hobza, P.; Müller-Dethlefs, K. *Non-Covalent Interactions: Theory and Experiment*; RCS Publishing: London, 2010.
(78) Boys, S.; Bernardi, F. The calculation of small molecular interactions by the differences of separate total energies. Some procedures with reduced errors. *Mol. Phys.* **1970**, *19*, 553−566.
(79) Kim, K.; Jordan, K. D. Comparison of density functional and MP2 calculations on the water monomer and dimer. *J. Phys. Chem.* **1994**, *98*, 10089−10094.
(80) Feyereisen, M. W.; Feller, D.; Dixon, D. A. Hydrogen bond energy of the water dimer. *J. Phys. Chem.* **1996**, *100*, 2993−2997.
(81) Jeffrey, G. A. *An Introduction to Hydrogen Bonding*; Oxford University Press: New York, 1997; Vol. *12*.
(82) Jurecka, P.; Sponer, J.; Cerny, J.; Hobza, P. Benchmark database of accurate (MP2 and CCSD(T) complete basis set limit) interaction energies of small model complexes, DNA base pairs, and amino acid pairs. *Phys. Chem. Chem. Phys.* **2006**, *8*, 1985−1993.
(83) Bates, D. M.; Tschumper, G. S. CCSD(T) Complete Basis Set Limit Relative Energies for Low-Lying Water Hexamer Structures. *J. Phys. Chem. A* **2009**, *113*, 3555−3559.
(84) Foulkes, W.; Mitas, L.; Needs, R.; Rajagopal, G. Quantum Monte Carlo simulations of solids. *Rev. Mod. Phys.* **2001**, *73*, 33−83.
(85) Pedulla, J.; Kim, K.; Jordan, K. Theoretical study of the n-body interaction energies of the ring, cage and prism forms of $(H2O)_6$. *Chem. Phys. Lett.* **1998**, *291*, 78−84.
(86) Santra, B.; Michaelides, A.; Fuchs, M.; Tkatchenko, A.; Filippi, C.; Scheffler, M. On the accuracy of density-functional theory exchange-correlation functionals for H bonds in small water clusters. II. The water hexamer and van der Waals interactions. *J. Chem. Phys.* **2008**, *129*, 194111.
(87) Bernal, J. D.; Fowler, R. H. A Theory of water and ionic solution, with particular reference to hydrogen and hydroxyl ions. *J. Chem. Phys.* **1933**, *1*, 515−548.
(88) Hamann, D. R. H_2O hydrogen bonding in density-functional theory. *Phys. Rev. B: Condens. Matter Mater. Phys.* **1997**, *55*, R10157−R10160.
(89) Kolb, B.; Thonhauser, T. Van der Waals density functional study of energetic, structural, and vibrational properties of small water clusters and ice I_h. *Phys. Rev. B: Condens. Matter Mater. Phys.* **2011**, *84*, 045116.
(90) Santra, B.; Klimeš, J.; Tkatchenko, A.; Alfè, D.; Slater, B.; Michaelides, A.; Car, R.; Scheffler, M. On the accuracy of van der Waals inclusive density-functional theory exchange-correlation functionals for ice at ambient and high pressures. *J. Chem. Phys.* **2013**, *139*, 154702.
(91) Hobbs, P. V. *Ice Physics*; Oxford University Press: Oxford, U.K., 1974.
(92) Whalley, E. Energies of the phases of ice at zero temperature and pressure. *J. Chem. Phys.* **1984**, *81*, 4087−4092.
(93) Hayward, J. A.; Reimers, J. R. Unit cells for the simulation of hexagonal ice. *J. Chem. Phys.* **1997**, *106*, 1518−1529.
(94) Murnaghan, F. The compressibility of media under extreme pressures. *Proc. Natl. Acad. Sci. U. S. A.* **1944**, *30*, 244−247.
(95) Brill, v. R.; Tippe, A. Gitterparameter von Eis I bei tiefen Temperaturen. *Acta Crystallogr.* **1967**, *23*, 343−345.
(96) Yoshimura, Y.; Stewart, S. T.; Somayazulu, M.; Mao, H.-k.; Hemley, R. J. High-pressure X-ray diffraction and Raman spectroscopy of ice VIII. *J. Chem. Phys.* **2006**, *124*, 024502.
(97) Nosé, S. A unified formulation of the constant temperature molecular dynamics methods. *J. Chem. Phys.* **1984**, *81*, 511−519.
(98) Hoover, W. G. Canonical dynamics: equilibrium phase-space distributions. *Phys. Rev. A: At., Mol., Opt. Phys.* **1985**, *31*, 1695−1697.
(99) Martyna, G. J.; Tobias, D. J.; Klein, M. L. Constant-pressure molecular-dynamics algorithms. *J. Chem. Phys.* **1994**, *101*, 4177−4189.
(100) Soper, A. K. Water and ice structure in the range 220−365 K from radiation total scattering experiments. 2014, arXiv:1411.1322.

DOI: 10.1021/acs.jpcb.6b03876
J. Phys. Chem. B 2016, 120, 7456−7470

(101) Morrone, J. A.; Car, R. Nuclear quantum effects in water. *Phys. Rev. Lett.* **2008**, *101*, 017801.
(102) Ceriotti, M.; Fang, W.; Kusalik, P. G.; McKenzie, R. H.; Michaelides, A.; Morales, M. A.; Markland, T. E. Nuclear quantum effects in water and aqueous systems: experiment, theory, and current challenges. *Chem. Rev.* **2016**, *116*, 7529−7550.
(103) Marsalek, O.; Markland, T. E. *Ab initio* molecular dynamics with nuclear quantum effects at classical cost: Ring polymer contraction for density functional theory. *J. Chem. Phys.* **2016**, *144*, 054112.
(104) Gasparotto, P.; Hassanali, A. A.; Ceriotti, M. Probing defects and correlations in the hydrogen-bond network of *ab initio* water. *J. Chem. Theory Comput.* **2016**, *12*, 1953−1964.
(105) Mills, R. Self-diffusion in normal and heavy water in the range 1−45.deg. *J. Phys. Chem.* **1973**, *77*, 685−688.
(106) Krynicki, K.; Green, C. D.; Sawyer, D. W. Pressure and temperature dependence of self-diffusion in water. *Faraday Discuss. Chem. Soc.* **1978**, *66*, 199−208.
(107) Skinner, L. B.; Huang, C.; Schlesinger, D.; Pettersson, L. G. M.; Nilsson, A.; Benmore, C. J. Benchmark oxygen-oxygen pair-distribution function of ambient water from X-ray diffraction measurements with a wide Q-range. *J. Chem. Phys.* **2013**, *138*, 074506.
(108) Soper, A. K. Joint structure refinement of X-ray and neutron diffraction data on disordered materials: application to liquid water. *J. Phys.: Condens. Matter* **2007**, *19*, 335206.
(109) Hura, G.; Sorenson, J. M.; Glaeser, R. M.; Head-Gordon, T. A high-quality X-ray scattering experiment on liquid water at ambient conditions. *J. Chem. Phys.* **2000**, *113*, 9140−9148.
(110) Soper, A. K. The radial distribution functions of water as derived from radiation total scattering experiments: is there anything we can say for sure? *ISRN Phys. Chem.* **2013**, *2013*, 279463.
(111) Soper, A. The radial distribution functions of water and ice from 220 to 673 K and at pressures up to 400 MPa. *Chem. Phys.* **2000**, *258*, 121−137.
(112) Soper, A. K.; Bruni, F.; Ricci, M. A. Site-site pair correlation functions of water from 25 to 400 °C: revised analysis of new and old diffraction data. *J. Chem. Phys.* **1997**, *106*, 247−254.
(113) Saitta, A. M.; Datchi, F. Structure and phase diagram of high-density water: The role of interstitial molecules. *Phys. Rev. E: Stat. Phys., Plasmas, Fluids, Relat. Interdiscip. Top.* **2003**, *67*, 020201.
(114) Skinner, L. B.; Galib, M.; Fulton, J. L.; Mundy, C. J.; Parise, J. B.; Pham, V.-T.; Schenter, G. K.; Benmore, C. J. The structure of liquid water up to 360 MPa from X-ray diffraction measurements using a high Q-range and from molecular simulation. *J. Chem. Phys.* **2016**, *144*, 134504.
(115) Dünweg, B.; Kremer, K. Molecular dynamics simulation of a polymer chain in solution. *J. Chem. Phys.* **1993**, *99*, 6983−6997.
(116) Yeh, I.-C.; Hummer, G. System-size dependence of diffusion coefficients and viscosities from molecular dynamics simulations with periodic boundary conditions. *J. Phys. Chem. B* **2004**, *108*, 15873−15879.
(117) Kestin, J.; Sokolov, M.; Wakeham, W. A. Viscosity of liquid water in the range − 8 to 150 °C. *J. Phys. Chem. Ref. Data* **1978**, *7*, 941−948.
(118) Pan, D.; Wan, Q.; Galli, G. The refractive index and electronic gap of water and ice increase with increasing pressure. *Nat. Commun.* **2014**, *5*, 53919.
(119) Costanzo, F.; Sulpizi, M.; Valle, R. G. D.; Sprik, M. The oxidation of tyrosine and tryptophan studied by a molecular dynamics normal hydrogen electrode. *J. Chem. Phys.* **2011**, *134*, 244508.
(120) Todorova, M.; Neugebauer, J. Extending the concept of defect chemistry from semiconductor physics to electrochemistry. *Phys. Rev. Appl.* **2014**, *1*, 014001.
(121) Freysoldt, C.; Neugebauer, J.; Van de Walle, C. G. Fully *ab initio* finite-size corrections for charged-defect supercell calculations. *Phys. Rev. Lett.* **2009**, *102*, 016402.
(122) Komsa, H.-P.; Rantala, T. T.; Pasquarello, A. Finite-size supercell correction schemes for charged defect calculations. *Phys. Rev. B: Condens. Matter Mater. Phys.* **2012**, *86*, 045112.
(123) Freysoldt, C.; Grabowski, B.; Hickel, T.; Neugebauer, J.; Kresse, G.; Janotti, A.; Van de Walle, C. G. First-principles calculations for point defects in solids. *Rev. Mod. Phys.* **2014**, *86*, 253−305.
(124) Frenkel, D.; Smit, B. *Understanding Molecular Simulation: from Algorithms to Applications*; Academic Press: San Diego, 2002.
(125) Kirkwood, J. G. Statistical mechanics of fluid mixtures. *J. Chem. Phys.* **1935**, *3*, 300−313.
(126) Kim, J.; Schmitt, U. W.; Gruetzmacher, J. A.; Voth, G. A.; Scherer, N. E. The vibrational spectrum of the hydrated proton: Comparison of experiment, simulation, and normal mode analysis. *J. Chem. Phys.* **2002**, *116*, 737−746.
(127) Trasatti, S. The absolute electrode potential: an explanatory note (Recommendations 1986). *Pure Appl. Chem.* **1986**, *58*, 955−966.

DOI: 10.1021/acs.jpcb.6b03876
J. Phys. Chem. B 2016, 120, 7456−7470